Medicine in Novel Technology and Devices 22 (2024) 100298

Contents lists available at ScienceDirect

Medicine in Novel Technology and Devices

journal homepage: www.journals.elsevier.com/medicine-in-novel-technology-and-devices/

Biomechanical analysis of bone mesoscopic structure and mechanical properties of vertebral endplates of degenerated intervertebral discs in rabbits

Bingying Zhao [a], Yuan Guo [a,*], Xushu Zhang [a], Yibo Zhao [b,**], Bin Zhao [b], Ming Zhang [c,***]

[a] College of Biomedical Engineering, Taiyuan University of Technology, Taiyuan, 030024, China
[b] The Second Hospital of Shanxi Medical University, Taiyuan City, 030001, China
[c] Department of Biomedical Engineering, Faculty of Engineering, The Hong Kong Polytechnic University, Hong Kong, 999077, China

ARTICLE INFO

Keywords:
Vertebral endplate
Biomechanics
Intervertebral disc degeneration model
Mechanical properties
Mesoscopic structure

ABSTRACT

In previous studies of disc degeneration, the structural and mechanical properties of the endplate were often neglected. In this paper, the station legislation was used to construct an animal model of minor trauma disc degeneration, and the mechanism of disc degeneration was further investigated by observing the changes of mesoscopic structure and developing the mechanical properties of endplate bone.

Twenty-eight 6-month-old Japanese white rabbits were divided into two groups: control group and experimental group. An animal model of intervertebral disc degeneration was established by upright experiment in the experimental group. The bone mesoscopic structures in different areas of each endplate were observed by histological and imaging methods, and the mechanical properties of the endplates were measured by indentation method. The two groups of data were compared by one-way ANOVA.

After the experimental animals stood for 17 weeks, The experimental group showed the characteristics of early disc degeneration. The microstructure of the degenerative group showed that the end plate mineralization degree was higher, the bone mass was larger, and the number and thickness of bone trabeculae were larger. The results of indentation test showed that the mechanical properties of the degeneration group were enhanced, and the lower endplate was obviously enhanced.

We successfully established a model of human disc degeneration with non invasive trauma and more consistent with the process of human disc degeneration through the standing experiment. In the experimental group, the internal structure of the endplate was dense and pore distance was reduced. The change of bone mesoscopic structure further affects the endplate, resulting in the enhancement of the mechanical properties of the endplate after intervertebral disc degeneration. The reduction of the pore distance and the narrowing of the internal channel structure of the endplate also hinder the nutrition supply of the intervertebral disc, which may be the key reason affecting the degeneration of the intervertebral disc. A biomechanical method for investigating the mechanism of intervertebral disc degeneration can be provided in this paper.

1. Introduction

The spinal intervertebral disc was a hydrated tissue whose physiological structure includes the nucleus pulposus, annulus fibrosus and endplates. The normal state of the intervertebral disc provides mechanical support for the stability of the spine [1,2]. If the intervertebral disc degenerates, the hydration capacity was reduced, resulting in dehydration of the intervertebral disc [3]. In the early stage of degeneration [4], the stability of the intervertebral disc segment may be lost. Intervertebral disc degeneration can lead to spinal instability and intervertebral disc herniation, which seriously affects the quality of life [2] and increases the economic burden. Some scholars believe that abnormal compressive stress was one of the important factors leading to intervertebral disc degeneration [5]. The intervertebral disc is mainly subjected

* Corresponding author.
** Corresponding author.
*** Corresponding author.
E-mail addresses: guoyuan@tyut.edu.cn (Y. Guo), zhaoyibo11@126.com (Y. Zhao), ming.zhang@polyu.edu.hk (M. Zhang).

https://doi.org/10.1016/j.medntd.2024.100298
Received 2 October 2022; Received in revised form 17 January 2024; Accepted 21 March 2024

to compressive stress. Excessive stress will have a negative impact on the nutritional supply and metabolism of the intervertebral disc, destroy the nutritional supply of the intervertebral disc, reduce the internal matrix content of the intervertebral disc, and accelerate the occurrence of intervertebral disc degeneration [6,7]. Studies have shown that intervertebral disc dystrophy is the ultimate cause of intervertebral disc degeneration [6,8,9]. The vertebral body endplate is the channel for supplying the intervertebral disc and plays an important role in the nutrient transport of the intervertebral disc. Seventy-five percent of the normal intervertebral disc nutritional supply instability comes from the endplate pathway [8]. Researchers believe that the supply of intervertebral disc nutrition comes from the vascular channels inside the endplate [10].

The integrity of the vertebral body endplate is beneficial to maintain normal intervertebral disc physiology. The vertebral body endplate and the adjacent intervertebral disc share the axial stress of the spine, which is extremely important to maintain the stability of the spine. If the intervertebral disc is subjected to high stress load for a long time, the nucleus pulposus may protrude into the endplate, the endplate will protrude axially, rupture, and the physiological state of the endplate will degenerate [11]. During this process, the structure of the annulus fibrosus of the intervertebral disc is disordered, and the intervertebral disc shows a degeneration state. The degree of degeneration increases with the increase of high-load stress, and the degeneration of the endplate also exacerbates the degeneration of the intervertebral disc [12]. Therefore, to study the changes of mesoscopic structure and mechanical properties of endplate during intervertebral disc degeneration is helpful to understand the mechanism of endplate degeneration.

At present, there are three main types of animal models for intervertebral disc degeneration: The first is that the injection of bone cement blocks the supply of nutrients to the disc, leading to degeneration [5]. The second type is the injury model.Koichi [6] established a model of disc degeneration by inducing the destruction of disc tissue by acupuncture. Surgery destroys ligaments and other tissues [7] and causes disc degeneration. The third type is abnormal stress-induced intervertebral disc degeneration. Hee [8]applied load loading force to the lumbar spine of New Zealand rabbits and established disc degeneration model. The establishment of these intervertebral disc degeneration models is often accompanied by greater trauma, which may affect the animal's own health state and thus affect the experimental results. in this paper, according to the method of Bai Xuedong [9], the experimental subjects were not subjected to any trauma, and the spinal column of experimental animals was subjected to stress for a fixed period of time every day to establish an animal model of non-invasive disc degeneration.

The height of the intervertebral space is an effective indicator to reflect the degree of intervertebral disc degeneration. Previous studies have shown that the degeneration of the intervertebral disc is accompanied by a decrease in the height of the intervertebral space [6]. Histological staining method is an important means to verify the degenerative changes of the intervertebral disc, and the results can directly reflect the number and state of cells in the intervertebral disc. Schneiderman's [13] method used T2WI image grayscale to quantitatively analyze the hydration state changes of the nucleus pulposus of the intervertebral disc, which can be used for the assessment of early degeneration of the intervertebral disc. At the same time, it overcomes the subjectivity of traditional grading. In this experiment, the degenerative state of the intervertebral disc will be comprehensively evaluated from three perspectives, including intervertebral space height (DHI), relative gray level of nucleus pulposus and histological staining.

Grant [14] et al., conducted indentation experiments with a 3 mm spherical indenter. Different regions of the end plate were found to have different mechanical properties. The destruction load in the lateral region of the upper lumbar endplate was 2.5 times greater than that in the central region. The stiffness of the edge region is greater than that of the middle region.The bearing capacity of the sacral endplate is better than that of the lumbar endplate. Cheng [15] et al., found that the mechanical strength of the bone endplate was reduced by grinding a certain thickness of bone endplate in indentation load test. In the vertebral body-intervertebral disc-vertebral body segment compression test by Zhao et al. [16], axial compression can lead to rupture of the endplate and damage to the trabecular bone structure. Hee [8] and others used an extracorporeal device to apply axial pressure on the L4-L5 of living white rabbits. After 28 days, they found that the channel structure of the endplate was reduced, accompanied by slight fractures. After the intervertebral disc degeneration, there have been no reports on whether there is a relationship between the mechanical environment change and the internal structure change, and whether the changes in mechanical properties in different regions of endplate are the same. Therefore, the study of the relationship between the mechanical properties of the normal and degenerative intervertebral disc endplate and the bone mesoscopic structure is conducive to the study of the mechanism of intervertebral disc degeneration.

The purpose of this paper is to construct an animal model of intervertebral disc degeneration with small trauma, which is closer to the process of human intervertebral disc degeneration. A variety of assessment methods were used to objectively determine whether the intervertebral disc was degenerative. The bone mesoscopic structure parameters of the corresponding regions inside the vertebral body endplate were observed. The elastic modulus, stiffness and hardness of endplate in the experimental group and the control group were obtained by indentation test. The correlation between the bone mesoscopic structure and mechanical properties of the intervertebral disc end-plate in the experimental group and the control group was analyzed. We assumed that the experiment could successfully establish the intervertebral disc degeneration model, and obtained the mechanical properties and bone microstructure changes of endplate before and after intervertebral disc degeneration.The research methods and results are contributive to understanding the mechanism of intervertebral disc degeneration.

2. Materials and methods

2.1. Establishment of intervertebral disc degeneration model

The bone structure of 6-month-old rabbits no longer grows and develops, which excludes the influence of growth factors on bone structure changes. Therefore, Twenty-eight 6-month-old Japanese white male rabbits, weighing 3 kg ± 0.25 kg, were randomly divided into two batches, the control and the experimental group. An animal model of intervertebral disc degeneration was established by upright standing experiment (Fig. 1) in the experimental group. If the rabbit's weight was too small, it can be fixed with a PVC plastic tube, and there is a mesh cover on the top of the device to prevent it from jumping out. A five-day adaptation period was set before the formal experiment, and the experimental group gradually adapted to the upright state. After five-day, the rabbits of experimental group stood in the upright device for 6 h a day, 9:00–12:00, 14:00–17:00, respectively. Except for the standing time, the rabbits of experimental group were kept in the cage for the rest of the time and could move freely as the same as the control group. After 17 weeks, animals were reared in a standardized manner, and handled in accordance with the principles of animal ethics in Taiyuan University of Technology.

2.2. Evaluation of intervertebral disc state

The intervertebral disc state was evaluated with three assessment methods, including histological morphology, intervertebral space height and relative gray level of nucleus pulposus. Histological morphology was assessed by HE staining. The height of intervertebral space and the relative gray level of nucleus pulposus were measured in software Mimics (Materialise corporation, Belgium, 19.0).

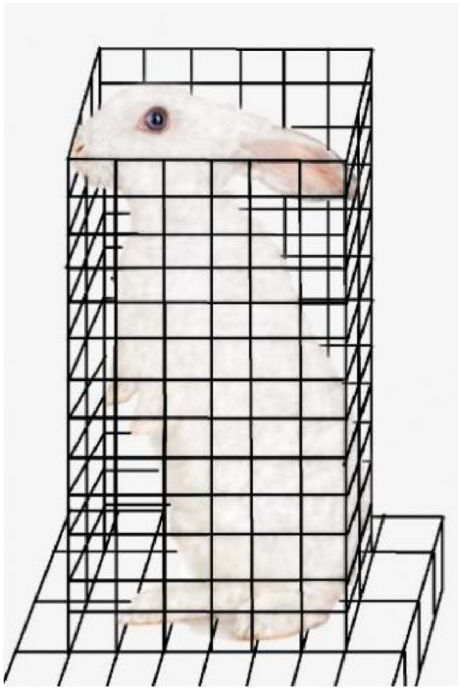

Fig. 1. Animal upright schematic graph.

2.2.1. Histological morphology

The purpose of histomorphological observation was to determine the physiological state and changes of the nucleus pulposus, annulus fibrosus, and endplates of the intervertebral disc, and to verify the intervertebral disc state. A total of 3 animals were selected, and the first rabbit was taken from the control group, which was standardized feeding for 17 weeks and weighed 4.2 kg. The second and third rabbits s were all taken from the experimental group, standing for 8 and 17 weeks, respectively, with a body weight of 3.2 kg and 4.2 kg. The rabbits were sacrificed with artery air-embolism. The lumbar vertebrae of the rabbits were cut off and divided into various segments. One segment includes 1/2 upper vertebral body, intervertebral disc, and 1/2 lower vertebral body. 2. 6 segments L2/3, L3/4, L4/5, L5/6, and L6/7 of each rabbit were obtained, and the intervertebral disc tissue cannot be damaged during the anatomical process. The segments were placed in tissue fixative solution for 48 h. After fixation, they were placed in the prepared formic acid decalcification solution for a week, then the specimens were dehydrated in an automatic dehydrator, rinsed for 15 min. At last, they were dissected in the midsagittal position, 4 μm sections were embedded in paraffin, and stained with hematoxylin-eosin (HE). The histological changes of endplates and intervertebral discs were observed by light microscope.

2.2.2. Imaging assessment

A total of 4 animals were selected for imaging evaluation. The first animal was taken from the control group and was reared for 17 weeks and weighed 4.4 kg. The 2nd-4th animals were all taken from the experimental group, standing for 8 weeks and weighing 3.1 kg; standing for 12 weeks, weighing 3.5 kg; standing for 17 weeks, weighing 4.1 kg.

Before using MRI for imaging evaluation, the leg muscles of the experimental subjects were exposed one by one, and SU-MIAN-XIN was injected for intramuscular anesthesia at a dose of 0.2 ml/kg. After the subjects were in a stable state, chloral hydrate was anesthetized through the ear vein injection at a dose of 1–1.5 ml/kg. After 3 min, check that the subject's heartbeat was stable and there is no limb response, it can be confirmed that the animal has entered an anesthetized state, and the imaging evaluation can be started. The nuclear magnetic scanning equipment used in this study is Philips 1.5T scanning system, and the spine phased array coil was used to scan and image the sagittal lumbar spine of the three experimental animals in the lateral decubitus position and head-first approach.

Intervertebral space height was measured using the interactive medical imaging software Mimics 19.0, as shown in Fig. 2. The rabbit spine image was imported into mimics and the image contrast was adjusted to highlight the bony part of the vertebral body. We measured and calculated DHI (Intervertebral space height index) using softwar-e.The intervertebral space height was calculated by referring to the "three median line method" of Kim [17] and others, and the intervertebral space height index DHI was calculated by referring to the calculation method of Koichi [6] and others. On the imaging images, the heights of the anterior edge A, middle B and posterior edge C of the intervertebral space, the heights of the anterior edge D, middle E and posterior edge F of the vertebral body above the intervertebral disc, and the heights of the anterior edge G, middle H and posterior edge I of the vertebral body below the intervertebral disc were measured respectively.The intervertebral height index was defined as $DHI = 2 \times (A + B + C)/(D + E + F + G + H + I)$, and the DHI of the control group and the experimental group were measured respectively.

In Mimics 19.0 software, the grayscales of three 0.5 mm^2 areas in the center of the nucleus pulposus of the lumbar intervertebral disc MRI image were extracted respectively (Fig. 3), and the average grayscale m_1 of the nucleus pulposus area was calculated. 14 regions with cerebrospinal fluid area of 0.3 mm^2 were selected equidistant from top to bottom, the average gray value was calculated as the cerebrospinal fluid gray value m_0. The relative gray value (m_1/m_0) was obtained. The signal changes of the intervertebral disc nucleus pulposus of experimental animals at different standing time were analyzed, so as to reflect the degree of intervertebral disc degeneration.

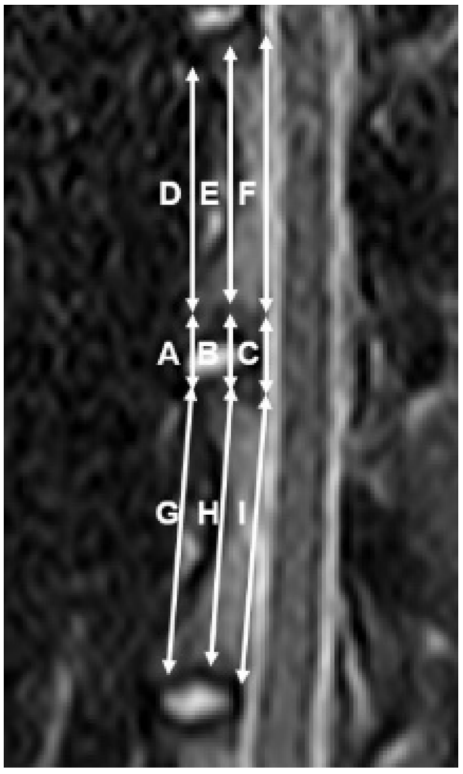

Fig. 2. DHI calculation method , The anterior margin of the intervertebral space is A, the middle height is B, and the posterior margin is C; the anterior margin of the vertebra above the intervertebral disc is D, the middle height is E, and the posterior margin is F; the anterior margin of the vertebra below the intervertebral disc is G, the middle height is H, and the posterior margin is I.

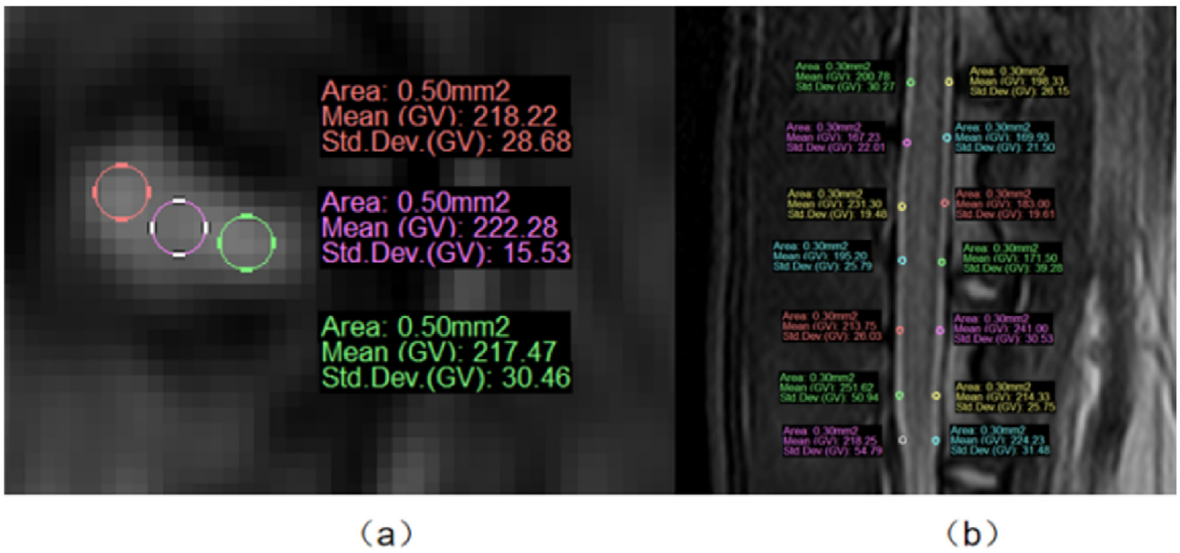

Fig. 3. Relative grayscale measurement (a) nucleus pulposus (b) cerebrospinal fluid.

2.3. Micro-CT scan

An animal standing for 17weeks in the experimental group and an animal of the same age in the control group were taken respectively. The rabbits weighed 4.2 kg and 4.0 kg, respectively. Before the experiment, the animals were sacrificed with artery air embolism. The tissue specimens acquisition method was the same as that in 2.2.1. The prepared specimens were fixed in 4% paraformaldehyde solution for 24–48 h, f washed three times with PBS (buffer solution), and were stored in 75% alcohol solution at 4 °C. Before starting the scan, the preserved tissue samples were first fixed, and the segments were placed in the rabbit standing three-dimensional position, and the Micro-CT (SkyScan1176, Bruker, Germany) scanning imaging system was used for scanning with a resolution of 18um. After scanning the vertebral body endplate images, import them into CTan software in BMP format for analysis. Six measurement regions from the upper and lower vertebral body endplates were selected, and each region was a 2 mm diameter circle with the center point as the center, and the region thickness was 1 mm. The center of each measurement region was the center point for subsequent indentation experiments. The center point of the measurement region was selected, as shown in Fig. 4. According to the definition of Martin [18] and others, the midsagittal plane and the coronal plane of the vertebral body endplate were determined. The sagittal diameter (AP) and transverse diameter (LR) of the upper and lower endplates of each vertebral body were measured sequentially using electronic digital calipers. The LR were marked with lines at 25%, 50% and 75%, and at the 25% and 75% of the AP. There were 6 overlapping points of the lines, namely A1, A2, A3, P1, P2 and P3, which were the center point of each measurement region.

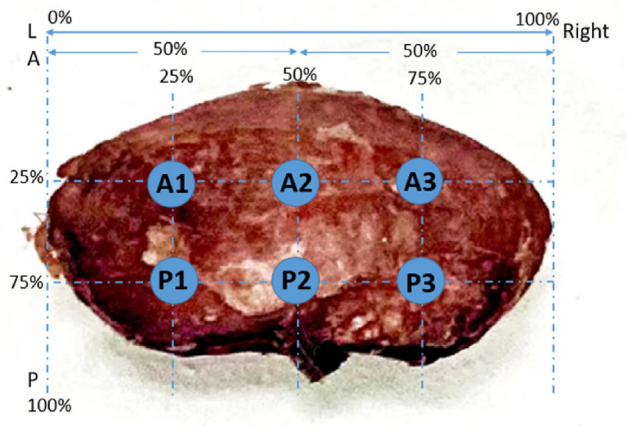

Fig. 4. Selection of 6 measure regions. Marks were made at 25%, 50% and 75% of the transverse diameter, and marks were made at 25% and 75% of the anterior and posterior diameters. There were six overlapping points, namely A1, A2, A3, P1, P2 and P3 (Figs. 3–5). The six points were used as the indentation area of the endplate. The vertebral endplate was divided into three equal parts according to the transverse diameter and two equal parts according to the sagittal diameter, and the vertebral endplate was divided into six specimens.

2.4. Indentation experiment

After the animals in the experimental group stood for 17 weeks, 9 animals in the experimental group with a body weight of 3.9 kg ± 0.3 kg and 8 animals in the control group with a body weight of 3.8 kg ± 0.3 kg of the same age were selected for experiments respectively. Before the experiment, the animals were sacrificed by air embolization, and the vertebral bone tissue was exposed by dissection. Disconnect from the intervertebral disc, take out the lumbar vertebrae L1-L7, remove the soft tissue to expose the endplate, the whole process does not damage the endplate. A metal bone saw was used to break the 2–3 mm below the endplate of each vertebral body. Due to the inconsistent thickness of the endplate in different regions, in order to maintain structural integrity and avoid damage to the vertebral body endplate, the bone and vertebral endplate with a thickness of about 2 mm were taken out, including the endplate and some trabecular structures under the endplate. In order to analyze the mechanical properties of the endplate in different regions, the endplate was divided into multiple specimens in different regions. The region division was the same as the measurement region division in 2.3 in this paper. Each region was used as a test specimen, that was, a vertebral body endplate was divided into 6 test pieces. The test pieces were storaged in sample bags and placed in a low temperature environment of −20 °C.

According to the formulas of indentation test defined by Oliver Pharr [19], for an ideal Berkovich indenter, the equivalent cone half angle is 70.32°. When the indenter is in contact with the material, a is the radius of the contact surface, and the projected contact area at the maximum indentation depth is:

$$A_c = \pi a^2 = \pi(h_c \tan a)^2 = 24.56 h_c^2 \quad (1)$$

The contact depth is defined as h_c , and the calculation formula of h_c is:

$$h_c = h_{\max} - \varepsilon \frac{P_{\max}}{S} \tag{2}$$

Among them, the $h_{\max}$ is the maximum indentation depth, ε is a constant, which is related to the shape of the indenter, and the ε of the Berkovich indenter is 0.75, $P_{\max}$ is the maximum load in the indentation experiment, and s is the slope at the top of the curve in the unloading phase.

The modulus Er can be obtained according to the formula (3) , which is also called the reduced modulus :

$$E_r = \frac{\sqrt{\pi}}{2\beta} \frac{S}{\sqrt{A_c}} \tag{3}$$

Among them, $\beta = 1.034$, is a constant, and related to the shape of the indenter, for a Berkovich indenter. Based on the formula of the reduced elastic modulus, the elastic modulus of the tested material can be obtained:

$$\frac{1}{E_r} = \frac{1-\nu^2}{E} + \frac{1-\nu_i^2}{E_i} \tag{4}$$

in this formula, ν is the Poisson's ratio of the tested material, E is the elastic modulus of the tested material, ν_i is the Poisson's ratio of the indenter material, and E_i is the elastic modulus of the indenter material. $E_i = 200$ GPa, $\nu_i = 0.3$, Poisson's ratio of most materials is between 0.15 and 0.35, for bone tissue, Poisson's ratio ν is set to 0.25.

In the indentation experiment, the hardness of the material can be obtained:

$$H = \frac{P_{max}}{A_c} \tag{5}$$

Biological tissues are viscoelastic materials [20], and the mechanical properties of materials are related to time. When the bone tissue indentation experiment was performed, an unsmooth curve like a "nose" would appear at the top of the unloading stage, as shown in Fig. 5a, and the unsmooth curve would affect the calculation results. In order to eliminate this effect, Briscoe [21] held the maximum load for 10s during the indentation experiment to ensure that such a situation does not occur, as shown in Fig. 5b. In the biological tissue indentation experiment, the influence of viscoelasticity can be effectively eliminated by maintaining the maximum load of 3s [22]-120s [23]. The commonly used retention time of biological bone tissue materials was 10s, therefore, 10s retention time was selected in this paper.

Before the indentation experiment, the sample bone tissue was thawed for 12 h to ensure that the sample bone tissue was fully thawed. The sample bone tissue was placed on the loading platform of general material testing machine Instron5544 (Instron Corporation, USA), and the indentation experiment was carried out with a triangular indenter with a diameter of 1 mm. In this experiment, the displacement controlled loading method was used to load the indentation experiment, and the loading speed was set. The speed set by the indenter was 0.2 mm/min. Set the maximum displacement to 0.2 mm. The holding time at the maximum force is 10s, and the maximum load is set to 500 N. After the parameters were set, tests were carried out to ensure the normal operation of the experimental equipment, and experiments were carried out on the bone tissue of the endplate sample in the order of A1, A2, A3, P1, P2 and P3. The load diagram is shown in Fig. 5 (b).

2.5. Data processing

SPSS23 (IBM Corporation, USA) software was used to process the statistical data, expressed as mean ± standard deviation, multiple comparisons between groups were performed by one-way ANOVA, and variance homogeneity test was performed by Levene method. The homogeneity of variance was tested by LSD test, and the least significant difference was tested by Tamhani T2(M) method. The data did not conform to a normal distribution, and the nonparametric rank sum test was used to analyze significance, and the results were expressed as 25%, 50%, and 75% digits. Take $P < 0.05$ as the cutoff value for statistical significance.

Correlation analysis was performed on the relative gray level of nucleus pulposus, intervertebral space height index, and bone microstructure parameters and mechanical parameters. The data were normal, and Pearson correlation analysis was performed; skewed data was subjected to Spearman correlation analysis, and the results were analyzed. Expressed in terms of r value and p value, $p < 0.05$ was considered to have overall correlation between the two data, $0<|r|<0.2$ was considered to have very weak correlation or no correlation, $0.2\leq|r|<0.4$ was considered to be weakly correlated, $0.4\leq|r|<0.6$ considered moderate correlation, $0.6\leq|r|<0.8$ considered strong correlation, and $0.8\leq|r|<1$ considered extremely strong correlation.

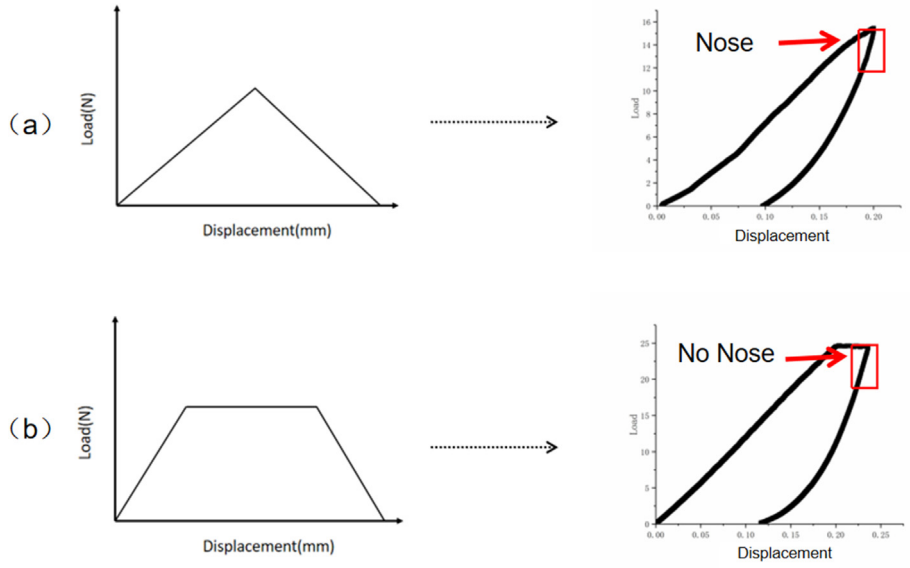

Fig. 5. Two loading methods of indentation experiment, (a) triangular loading (b) trapezoidal loading [21].

3. Results

3.1. Histological morphology results

Histological morphology of 8 and 17weeks standing in the experimental group and standardized feeding for 17 weeks in the control group, was shown in Fig. 6. The number of nucleus pulposus cells of the intervertebral disc was large and densely distributed, the annulus fibrosus were closely arranged and the number of cells was large in the control group. While in the experimental group, the number of nucleus pulposus cells were decreased for 8 weeks standing, the number of nucleus pulposus cells was less and the distribution gradually became sparser for 17 weeks standing. The nucleus pulposus of the intervertebral disc was swollen and protruded into the posterior annulus fibrosus. The nucleus pulposus cells were unevenly distributed, the matrix was uneven, and a few vacuolated cells appeared. In the experimental group, the annulus fibrosus structure was wavy, lost the concentric circular regular arrangement, the lamella was loose or even broken, and the degree of fibrosis was aggravated with he increase of standing time. Therefore, it could be indicated that the intervertebral disc entered a degeneration state after standing for 17 weeks in the experimental group.

3.2. Imaging assessment results

The average height of the intervertebral space (DHI) of the lumbar spine at 0 (the control group), 8, 12 and 17 weeks of standing was calculated respectively. As shown in Fig. 7a, DHI was 0.3192, 0.2629, 0.2319 and 0.2173, respectively. Compared with the control group, DHI was decreased by 17.63%, 27.34%, and 31.92% at 8, 12, and 17 weeks standing, respectively. As shown in Fig. 7b, the relative gray levels of the nucleus pulposus (m_1/m_0) at 0 (the control group), 8, 12 and 17 weeks of standing was 1.0061, 0.8844, 0.832, and 0.6651, respectively. Compared with the control group, it decreased by 12.10%, 17.30% and 33.89% respectively. According to the modified Pfirrmann [24] degeneration scale, a 30% reduction of the DHI can be considered as a degeneration of the intervertebral disc. Therefore, it could be concluded that the intervertebral disc was degenerated after standing for 17 weeks in the experimental group.

3.3. Micro-CT scan results

The comparison of the same (anterior, and posterior) regions between the control group and the experimental group was analyzed. The bone parameters of the upper endplate in the experimental group, the Tb.N value of the anterior region was significantly higher than that of the control group ($p < 0.05$), and the value of Tb.Sp was significantly lower than that in the control group ($p < 0.05$). The bone parameters of the lower endplate in the experimental group, the values of BV/TV and Tb.N in the posterior region of the experimental group were significantly higher than those of the control group ($p < 0.05$), and the value of Tb.Sp in the anterior region of the experimental group was significantly greater than that of the control group, and the posterior region was smaller than that of the control group ($p < 0.05$). The results showed that after intervertebral disc degeneration, the structure of trabecular bone in the anterior region of the upper endplate and the posterior region of the lower endplate changed significantly, the number of trabeculae increased, and the bone volume fraction increased.

The comparison of the same (left, middle and right) regions between

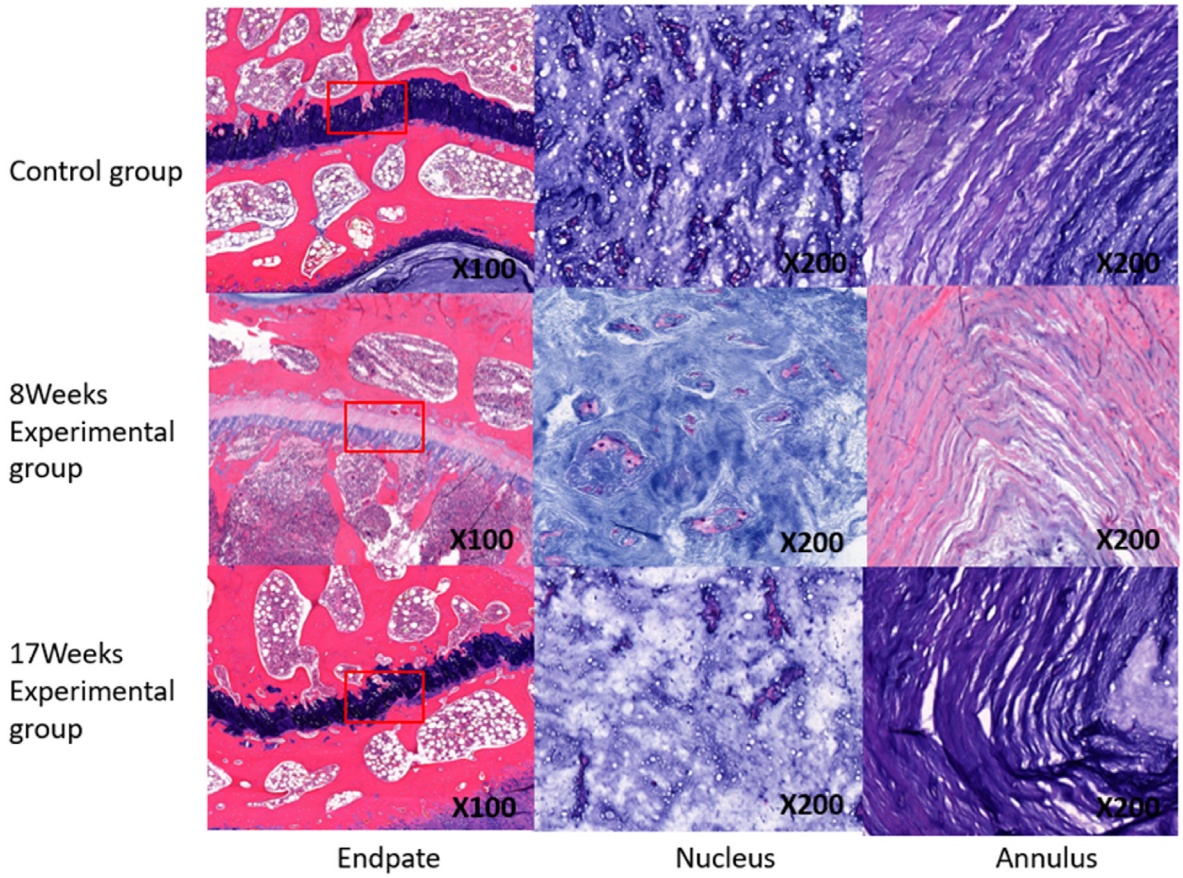

Fig. 6. Histological morphology of the control group, 8weeks and 17weeks of the experimental group. Note: Endplate refers to the structure of the vertebral endplate, Nucleus refers to the nucleus pulposus, Annulus refers to the annulus fibrosus of the intervertebral disc, × 100 refers to the observation under 100 times, and × 200 refers to the observation under 200 times.

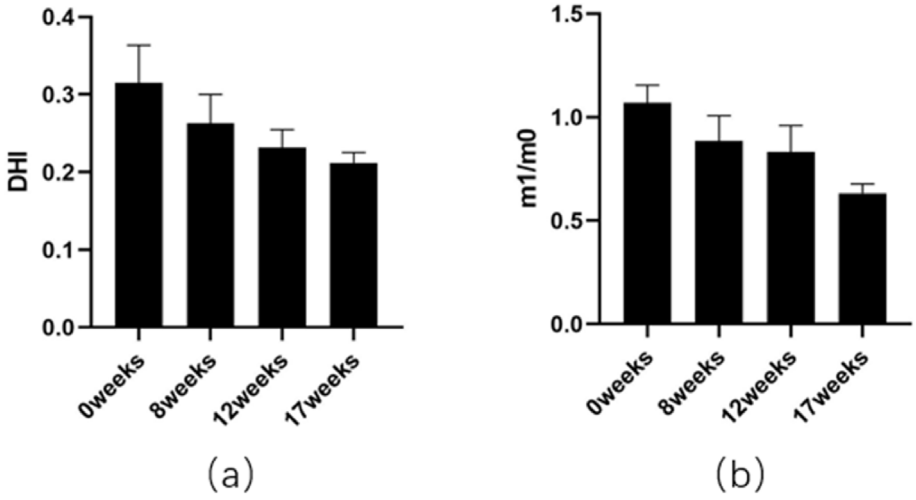

Fig. 7. Imaging index at different standing times (a) DHI (b) m1/m0 , The data were in mean ± standard deviation format.

the control group and the experimental group was analyzed. The bone parameters of the upper endplate, the values of BMD, BV/TV, Tb.Th and Tb.N in the middle region were greater than those in the left and right regions, and the value of Tb.Sp was smaller than the left and right regions. The bone parameters of the lower endplate in the experimental group, the values of BMD, BV/TV, Tb.Th and Tb.Sp in the middle region were greater than those of in the left and right regions, and Tb.N in the middle region was less, while the values of BMD、BV/TV、Tb.Th、Tb.N in the middle region in the control group were smaller than those of in the left and right regions ，and Tb.N in the middle region was. The results showed that after intervertebral disc degeneration, the bone structure in the medial region of the inferior endplate became denser, the spacing became smaller, the thickness was larger, and the bone volume fraction and bone mineral density were significantly greater than those on the left and right sides.

By analyzing the bone mesoscopic structure parameters of the lumbar endplates of 17 weeks standing in the experimental group and the control group of the same age (Fig. 8), it can be found that after the intervertebral disc degeneration, the BMD parameters of the vertebral body endplate was increased, indicating that the bone mineral density of the vertebral body endplate was increased, and the mineralization of bone tissue was increased. In the experimental group, BV/TV, TB.Th, and Tb.N, and of the vertebral body endplate was 44.6%, 141.9 μm, and 0.00321/μm, respectively, which was higher than 41.6%, 137.2um, and 0.00311/μm respectively in the control group. Tb.Sp of the experimental group was 244.9um, which was smaller than 262.6um of the control group. The Micro-CT images of the L2/3 segments of the control group and the experimental group (Fig. 9). It could be seen that the internal trabecular structure of the endplate was denser in the experimental group.

3.4. Indentation test results

3.4.1. Upper and lower endplate data of each segment

The mechanical properties of the upper and lower lumbar endplates of 17weeks standing in the experimental group and the control group of the same age were analyzed (Fig. 10). The *E* of the upper endplate of the L12, L34, L45, L56, and L67 segments of the experimental group was significantly greater than that of the control group ($p < 0.05$). *H* of the upper endplate of the L12, L45, and L56 experimental groups was significantly greater than that of the control group, and the hardness of the upper endplate of the L34 and L56 experimental groups was greater than that of the control group ($p < 0.05$), but not significant. *S* of the upper endplate of the L12, L34, L45, and L56 experimental groups was significantly greater than that of the control group ($p < 0.05$).

By comparing the lower endplate of the control group with the experimental group, it could be found from Fig. 11 that the *E*, *H*, and *S* of the lower endplate of each segment in the experimental group were significantly greater than those in the control group ($p < 0.05$).

3.4.2. Mechanical properties of different regions of the endplate

The *E*, *H*, *S* of the control group and the experimental group endplates were calculated, and the data were statistically analyzed.

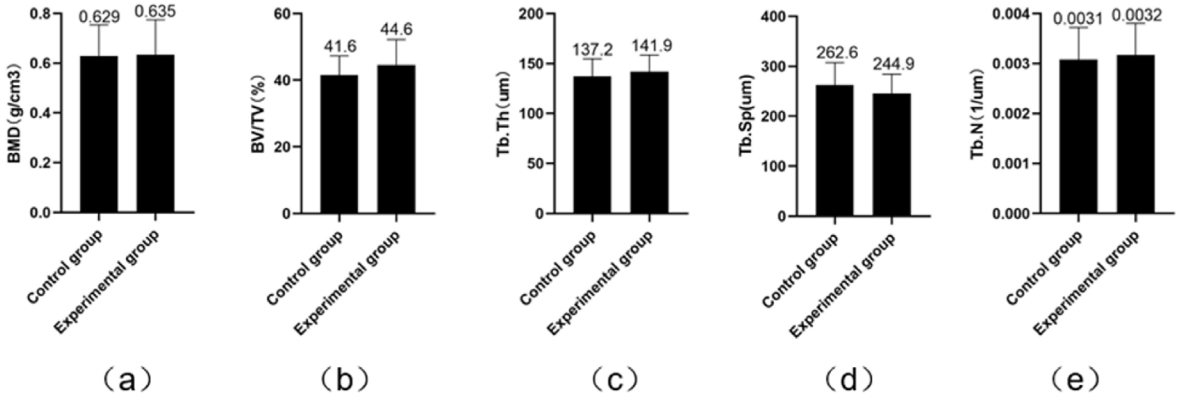

Fig. 8. Bone mesoscopic structure parameters of control group and experimental group (a) Bone mineral density BMD (b) Bone volume fraction BV/TV (c) Trabecular thickness Tb.Th (d) Trabecular separation Tb.Sp (e) Small bone Beam thickness Tb.N. The data were in mean ± standard deviation format.

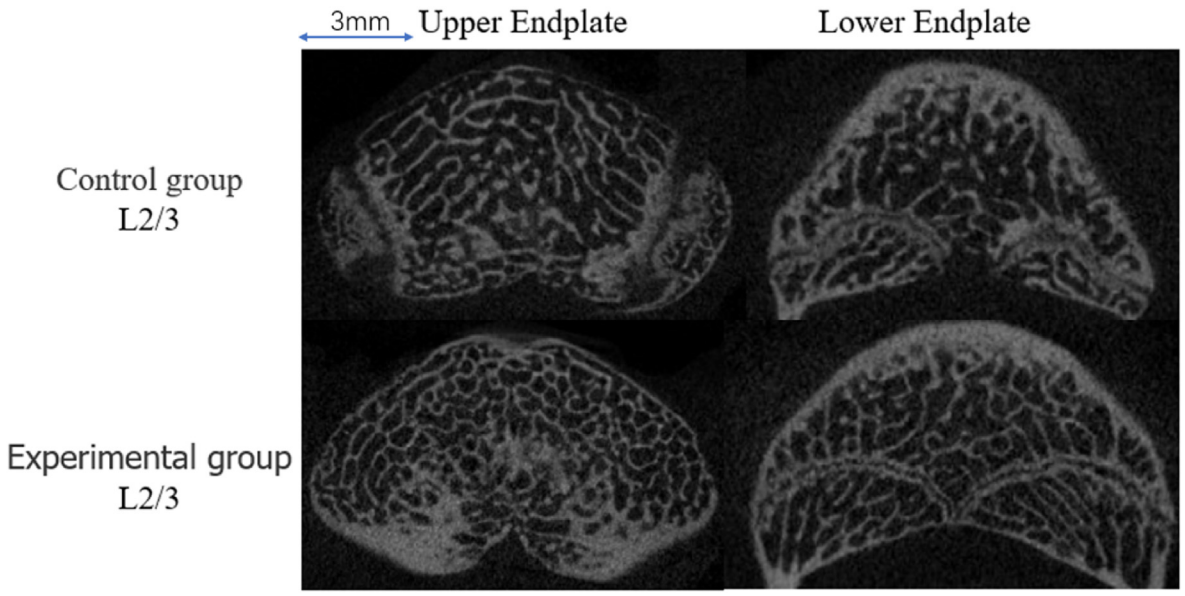

Fig. 9. Micro-CT images of the L2/3 segment in the control and experimental groups, 0.5 mm below the surface of the vertebral endplate.

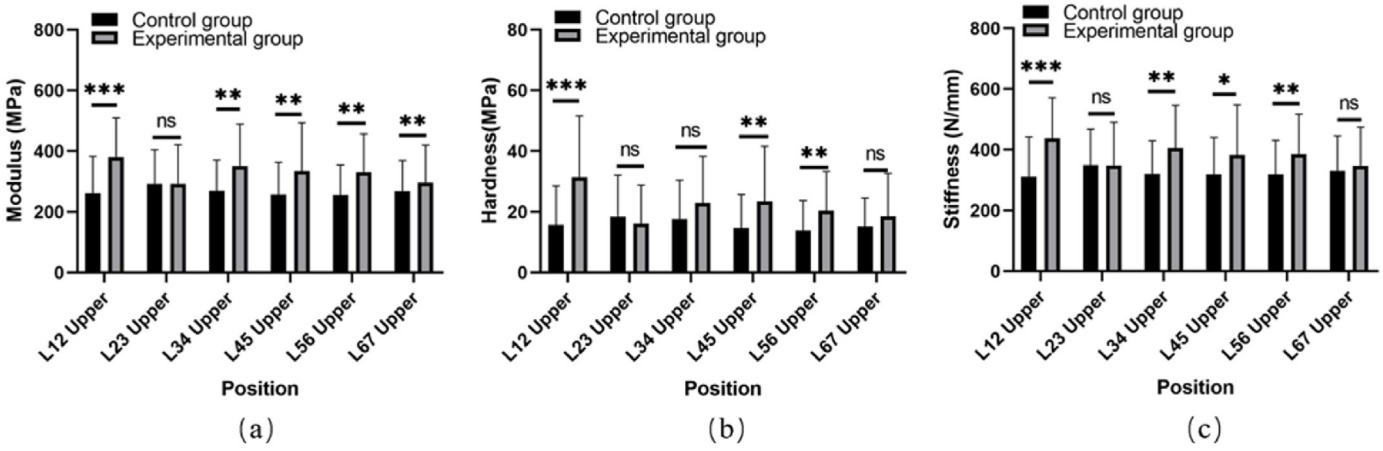

Fig. 10. The mechanical properties of each segment of upper endplate in the control and experimental group，(a) Elastic modulus (b) hardness (c) stiffness, * refers to $P < 0.05$, ** refers to $P < 0.01$, * * * refers to $P < 0.001$.The data were in mean ± standard deviation format.

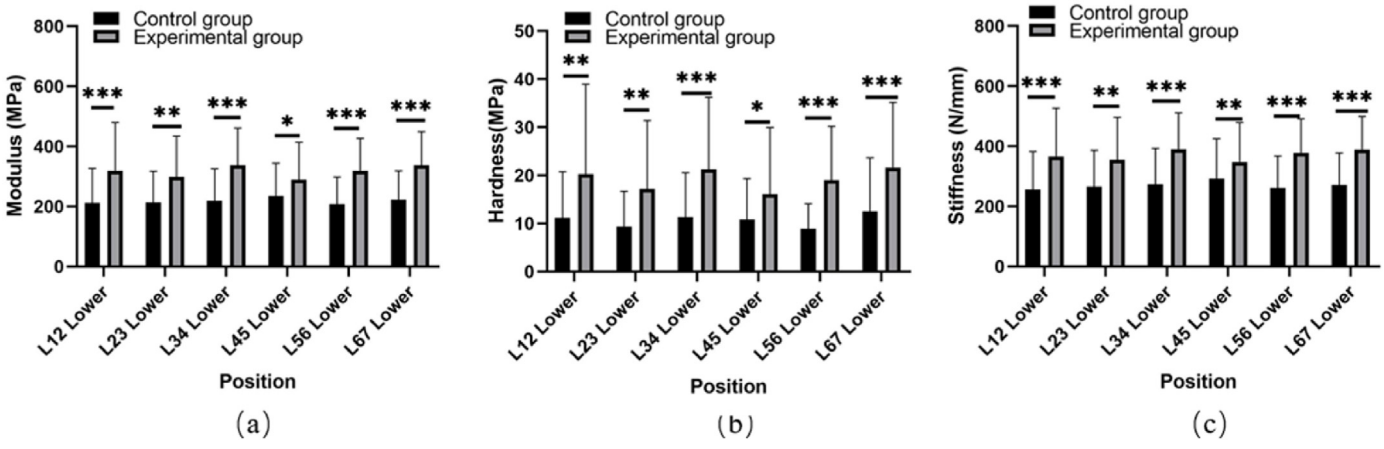

Fig. 11. The mechanical properties of each segment of Lower endplate in the control and experimentalgroup，(a) Elastic modulus (b) hardness (c) stiffness, * refers to $P < 0.05$, ** refers to $P < 0.01$, * * * refers to $P < 0.001$.The data were in mean ± standard deviation format.

3.4.2.1. Anterior and posterior regions of the upper and lower endplates. The mechanical properties in the anterior and posterior regions of the upper and lower endplates were compared. The values of the upper endplate were greater than those of the corresponding region of the lower endplate, but there was no statistical difference. For *E* and *S*, the values in the anterior region were greater than those in the posterior region, but there is no statistical difference, and for *H*, there is no obvious rule. The mechanical properties in the same regions of the control group and the experimental group were compared (Fig. 12). The data values of the experimental group was significantly greater than that of the control group ($p < 0.001$).

3.4.2.2. Left, middle and right regions of the upper and lower endplates. The mechanical properties in the left, middle and right sides of the upper and lower endplates were compared between the control group and the experimental group. The values of the upper endplate were greater than that of the corresponding regions of the lower endplate, but there was no statistical difference. As shown in Fig. 13, in the upper endplate of the control group, the values of *E* and *S* in the middle region were significantly greater than those on the left and right ($p < 0.05$), and for *H*, the values in the middle were significantly greater than those on the left ($p < 0.05$). In the lower endplate, the values in the middle region were larger, but there was no statistical difference. In the lower endplate of the experimental group, the values in the middle region were significantly greater than those on the left and right regions ($p < 0.05$), and in the upper endplate, the values in the middle region were larger, but there was no statistical difference. The mechanical properties in the same regions of the control group and the experimental group were compared.

3.4.2.3. Six different regions of the upper and lower endplates. The modulus, hardness and stiffness of 6 regions of the each endplate in the control group and the experimental group were compared. The change rate *R* was introduced, i.e. the relative rate of change *R* =(experimental group data - control group data)/control group data. $R > 0$ indicated that the experimental group was larger than the control group, while $R < 0$ indicated that the experimental group was smaller than the control group.

R of the *E*, *H*, and *S* was all greater than zero. The average values of *R* of the *E*, *H*, and *S* was 39%, 41%, and 26% in the upper endplate, respectively, and the average values of *R* was 45%, 82%, 38% in the lower endplate, respectively. *R* of the six regions of the upper and lower endplates was calculated, as shown in Fig. 14. For the upper endplate, *R* of *E*, *H*, *S* was the largest in the A1 region, while *R* was the smallest in the A2 region. For the lower endplate, *R* of *E*, *H*, *S* was larger in the A2 and P2, while *R* was the smallest in the P1. It could be seen that, the change of mechanical properties parameters of the lower endplate was larger than that of the upper endplate after intervertebral disc degeneration. Among the three parameters, the change rate of hardness was the largest and the

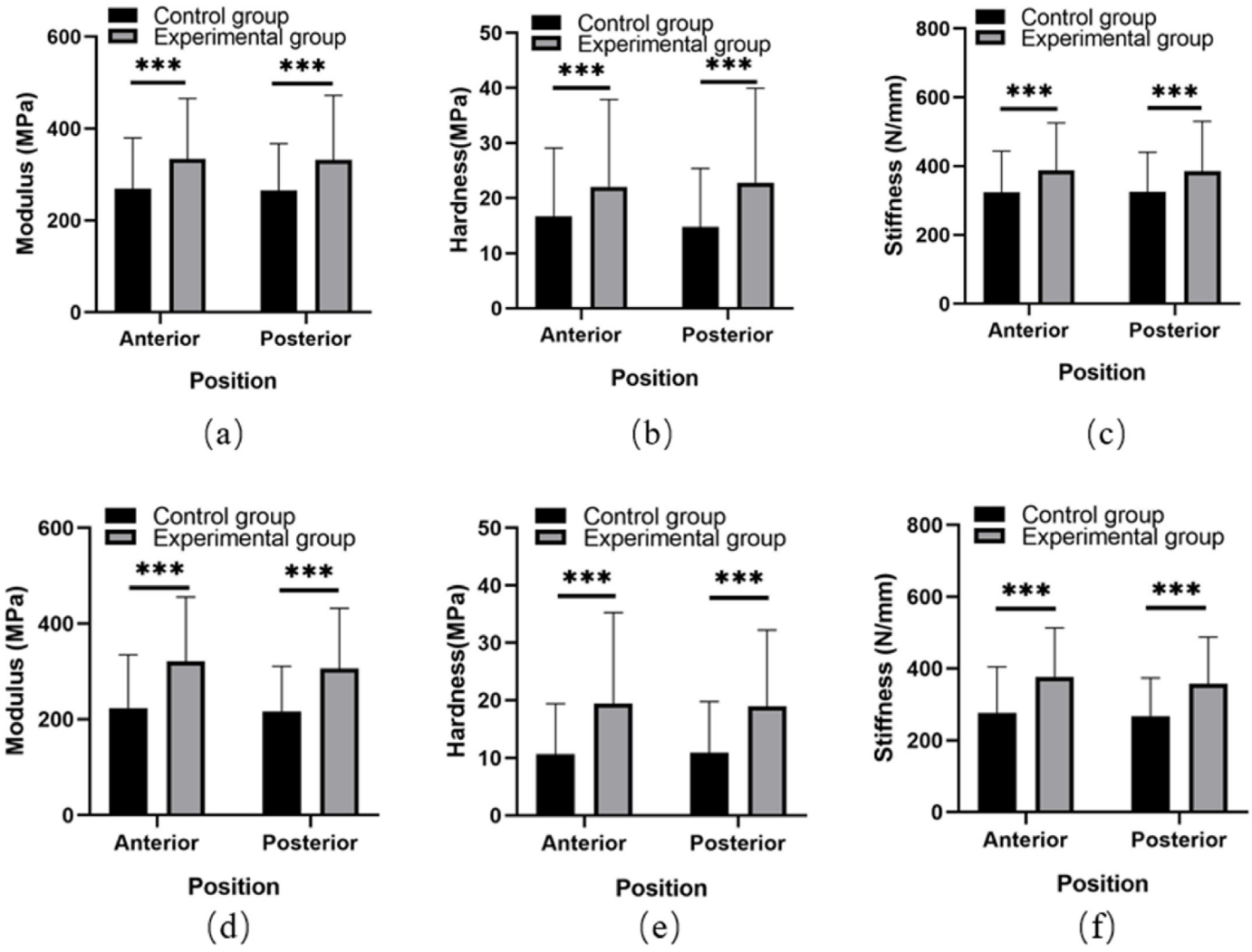

Fig. 12. Mechanical properties of the anterior and posterior regions of the endplate in the control and experimental groups. Upper endplate: (a) *E*, (b) *H*, (c) *S*, lower endplate: (d) *E*, (e) *H*, (f) *S*.The data were in mean ± standard deviation format.

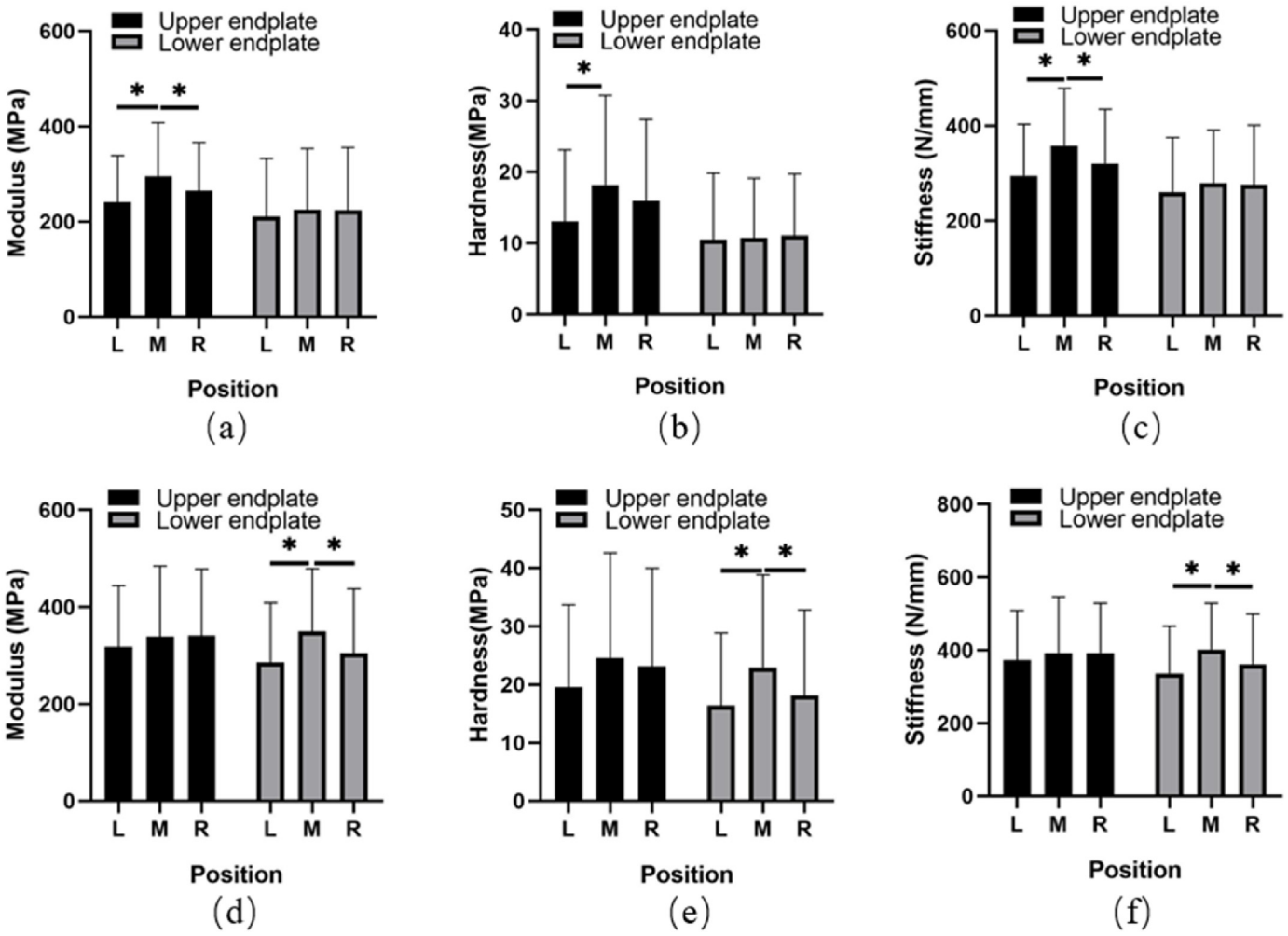

Fig. 13. Mechanical properties of the left, middle and right regions of the upper and lower endplates Control group: (a), (b), (c) Experimental group: (d), (e), (f).The data were in mean ± standard deviation format.

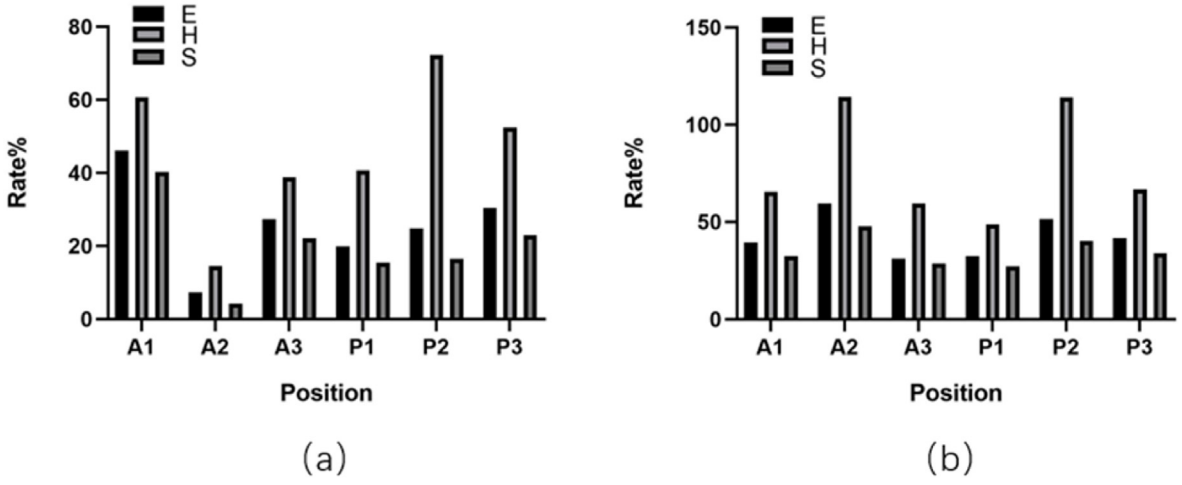

Fig. 14. Rate of change of elastic modulus, hardness and stiffness in six regions (a) upper endplate (b) lower endplate.

change rate of stiffness was the smallest in the six regions.

Statistical data were expressed as mean ± standard deviation, multiple comparisons between groups were performed by one-way analysis of variance, the variance homogeneity test was performed by Levene method, and the variance homogeneity test was performed by Welch and Brown-forsyth test, and the least significant difference method LSD test. If the variance is not uniform, the Tamhani T2 (M) method is used to test.

4. Discussion

In this study, an animal model of intervertebral disc degeneration with non invasive trauma was first constructed by upright experiment, and the intervertebral disc degeneration status was obtained by histological staining and imaging evaluation. The nucleus pulposus cells in the model group were not uniformly distributed and the matrix was uneven.The mechanical properties of endplate before and after intervertebral disc degeneration were obtained by indentation experiment, and the bone microstructure parameters of endplate before and after intervertebral disc degeneration were obtained by Micro-CT. The microstructure of endplate bone is dense and the pore distance is reduced. Through standing experiment, we successfully established a model of disc degeneration, and studied the mechanical properties of vertebral endplate and the changes of internal bone microstructure before and after disc degeneration. The changes of endplate in the process of intervertebral disc degeneration were further investigated, which provided a biomechanical method for studying the mechanism of intervertebral disc degeneration.

4.1. Establishment and evaluation of animal models of intervertebral disc degeneration

Among the many factors that affect intervertebral disc degeneration, abnormal compressive stress is considered to be an important factor [25]. The main function of the intervertebral disc is to bear compressive stress. Excessive stress will have a negative impact on the nutrient supply and metabolism of the intervertebral disc, resulting in the reduction of the content of matrix in the intervertebral disc and accelerating the occurrence of intervertebral disc degeneration [26]. At present, scholars generally believe that abnormal compressive stress destroys the nutrient supply of the intervertebral disc and accelerates the degeneration of the intervertebral disc [27]. Lotz [12] and others studied the effect of high load on the intervertebral disc tissue and found that under high load, the structure of the middle and inner annulus fibrosus of the intervertebral disc was disordered, and the occurrence of this disorder was aggravated with the increase of the load. Jing Jiefu [28] and others found that abnormal stress can affect the microstructure changes of the vertebral body, which can lead to instability of the cervical spine and accelerate the degeneration of the intervertebral disc. Revel [11] and others applied periodic stress stimulation to mice, and found that the thickness of the endplate became uneven, the nucleus pulposus protruded into the cartilage endplate, the endplate ruptured, and the degeneration of the endplate further aggravated the degeneration of the intervertebral disc. The reduction of nutrients was considered to be the ultimate cause of intervertebral disc degeneration [29]. Research [30,31]showed that the obstruction of intervertebral disc nutrition can cause intervertebral disc degeneration. In previous studies, the establishment of most intervertebral disc degeneration models is mostly based on the design of the spine under high load stress. A fixation device was installed in the adjacent vertebral body of the intervertebral disc, and an axial load was applied on the intervertebral disc to establish a degeneration model [11]. In the previous methods of intervertebral disc modeling, whether classical acupuncture or implantation of the loading device, will bring greater trauma to the experimental animals, and the injury may affect the health status of animal, which is inconsistent with the degeneration process of human intervertebral disc in the natural upright state, In this paper, a degeneration model of intervertebral disc was established based on the principle of intervertebral disc degeneration caused by compression, referring to the upright loading method used by Bai Xuedong [9] and others. By standing at different times every day, their own gravity exerted axial pressure on the intervertebral disc, which caused intervertebral disc degeneration. The establishment of degeneration model in the upright state was basically consistent with the process of human's intervertebral disc degeneration.

In magnetic resonance imaging, the gray value is proportional to the water content. After degeneration, the water content of the nucleus pulposus of the intervertebral disc is significantly reduced, and the gray value will also decrease accordingly. Pfirrmann grading is used widely in clinical to evaluate the degeneration grade based on the doctor's observation of the gray scale of the intervertebral disc. The improved Pfirrmann [24] grading and evaluation system, although the evaluation of intervertebral disc degeneration is more detailed, it is still a non-quantitative method to evaluate by the doctor's human eye. This traditional evaluation method inevitably has its own subjectivity [32]. Schneiderman's [13] and others evaluated the water content of the intervertebral disc by analyzing the grayscale of the magnetic resonance image, and made an objective evaluation of the degeneration of the intervertebral disc. This method can improve the accuracy of early disc degeneration assessment, and it is adopted in this paper. The state of the intervertebral disc in the experimental group and the control group were evaluated by histological and imaging methods. The results of histological morphology showed that the number of nucleus pulposus cells in the control group was normal, the cartilage endplate was not damaged, and the annulus fibrosus was arranged in an orderly manner (Fig. 6). In the experimental group, the nucleus pulposus cells of the intervertebral disc were reduced, the nucleus pulposus protruded into the endplate, the annulus fibrosus was disordered, the thickness of the endplate was reduced, and the structure of the endplate was slightly damaged; The imaging results showed that the height of the intervertebral space in the experimental group was smaller than that in the control group, and the longer the standing time, the smaller DHI (Fig. 7a) and m_1/m_0 (Fig. 7b). After standing for 17 weeks, DHI decreased by 31.92%, and m_1/m_0 decreased by 33.89% compared with the control group. In the classic stab wound model, after two weeks of modeling, the DHI decreased by 20%, and the intervertebral disc entered a state of degeneration [6]. m_1/m_0 of the nucleus pulposus at 17 weeks standing was 0.6651, which was close to m_1/m_0 of five patients with intervertebral disc degeneration and herniation listed by Dike [33] and others in the intervertebral disc transplantation. From the above results, standing to apply axial load to the intervertebral disc can cause early degeneration of the intervertebral disc. The results indicated that with the increase of standing time, DHI and m_1/m_0 gradually decreased, and the degree of degeneration gradually aggravated.

4.2. Bone mesoscopic structure of the endplate

The vertebral body endplate is a bony structure similar to bone tissue except for the surface cartilage endplate. The physiological demarcation between the vertebral endplate and the trabecular structure of the vertebral body is not well defined, which makes the detection of the vertebral endplate structure difficult [34,35]. It is difficult to standardize in the measurement of endplate mesoscopic structure [36]. Wang [37] and others used Micro-CT to scan 150 lumbar vertebrae (L1-L5) and measured the thickness of bony endplates and found that the average thickness of endplates was about 1 mm. Most scholars choose to measure the bone parameters of the 1–2 mm layer thickness below the surface of the vertebral endplate as the structural parameters of the endplate. Therefore, the ROI thickness selected was 1 mm in this paper. In the X-ray image, the endplate structure is convex around and concave in the central area [38]. There are more and more studies on the morphology of the vertebral endplate, and the results of other scholars believe that the endplate structure is a thin porous plate-like bone layer [39–43]. Tomonori [10] and others used Micro-CT scanning to observe the porous network structure inside the vertebral body endplate.

The findings suggest that the bone mesoscopic structure of the vertebral endplates maybe closely related to intervertebral disc degeneration [37,44–48]. Intervertebral disc degeneration may be related to structural sclerosis of vertebral endplate [49]. This suggests that the changes of bone mesoscopic structure in the vertebral endplates can be associated with the degeneration of intervertebral disc. Zhang Hengyan [50] and others established a scoliosis model by inserting bone screws in

mice, and observed that the microstructure in the endplate changed to varying degrees. The loading of the bony endplate will affect the internal vascular channel structure. Under the action of asymmetric force, the channel structure of the convex endplate is more developed, and the channel of the concave endplate is sparser. Changes in the number of channel structures may affect the transport efficiency of intervertebral disc nutrients. From the comparison of CT image, it can also be seen that the bone mesoscopic structure of the endplate in the control group was denser (Fig. 9) in this paper.

4.3. Mechanical properties of the endplate

The thickness of the bony endplate has an important influence on its own mechanical properties. Grant [14] found that the load-bearing capacity of the sacral endplate was better than that of the lumbar endplate through spherical indentation experiments, and the load-bearing capacity of the lower lumbar endplate was 40% higher than that of the upper endplate. Cheng [15] and others found through the indentation load test that the ultimate stress of the intact bony endplate was 106 N. Decreased mechanical strength of bony endplates with a certain thickness removed, and the ultimate stress of the bony endplate after grinding 1 mm was reduced to 59 N, with an average loss of 44%, the ultimate stress of the bony endplate with a 2 mm resection was reduced to 51 N, with an average loss of 52%. Therefore, the thickness of the bony endplate is crucial to maintain its mechanical properties. By studying the mechanical properties of vertebral endplates of the control group and the experimental group, it is beneficial to penetrate the role of endplates in intervertebral disc degeneration. At present, nanoindentation experiment is basically used to measure the mechanical properties of vertebral endplates, from the microscopic point of view. In the analysis, the influence of the defect of bone tissue, the uneven thickness of the endplate and the trabecular bone structure under the vertebral endplate is ignored. In the experiments of other scholars, using traditional mechanical testing methods, i.e. compression test, the mechanical properties of the whole endplate can be obtained, and the mechanical properties of different regions of the endplate cannot be accurately obtained. The research results of other scholars showed that the stiffness of the endplate was different in different regions, and the stiffness of the endplate was higher in the posterior position [51]. The results of spherical indentation experiments show that the mechanical properties of the vertebral endplate are related to its own thickness, and the greater the thickness, the stronger the mechanical properties [15]. It showed that the mechanical properties of the vertebral body endplates were spatially different.

4.4. Effect of degeneration on endplate

In order to explore the relationship between the mesoscopic structure of bone and the mechanical properties of the endplate before and after intervertebral disc degeneration, the correlation between the mechanical properties of each vertebral body and m1/m0, DHI and mesoscopic structure parameters of bone was analyzed.

The results showed that *E*, *H*, *S* were moderately negatively correlated with m1/m0, respectively ($r = -0.5192$, $P < 0.001$, $r = -0.4269$, $P < 0.001$, $r = -0.5059$, $P < 0.001$) respectively. There was a moderate negative correlation between the *E*, *H*, *S* and DHI ($r = -0.498$, $P < 0.001$, $r = -0.4192$, $P < 0.001$, $r = -0.4864$, $P < 0.001$) respectively. The analysis between bone microstructural parameters and mechanical parameters showed that there was a weak negative correlation between *E*, *H* and the bone trabecular separation. While there was a weak positive correlation between *E*, *H* and the Bone mineral density BMD, bone volume fraction BV/TV, bone trabecular number Tb.N, which is consistent with the results found by Mulder [52] and other. The changes in *E* may be related to the mineralization content of bone tissue [53].

The correlation between *E* and BV/TV of different segments was analyzed(Fig. 15), there was a strong positive correlation in L5/6 segment ($r = 0.6072$, $P < 0.01$). There were moderate positive correlations in L1/2 and L4/5 segments ($r = 0.4367$, $P < 0.05$; $r = 0.5295$, $P < 0.01$). There was no correlation in L2/3 and L3/4 segments. The correlation between *E* and BMD of different segments was analyzed(Fig. 16), there was a strong positive correlation in L5/6 segment ($r = 0.6447$, $P < 0.001$). There was a moderate correlation in L4/5 segment ($r = 0.5577$, $P < 0.01$). There was no correlation in L1/2 segment, L2/3 segment and L3/4 segment. This indicates that the degeneration is more severe in the lower segment of the spine.

5. Conclusion

An intervertebral disc degeneration model with non invasive trauma and more in line with the process of human intervertebral disc degeneration was successfully established in this paper. The intervertebral disc degeneration was objective evaluated using a variety of evaluation methods. The bone mesoscopic structure parameters of the

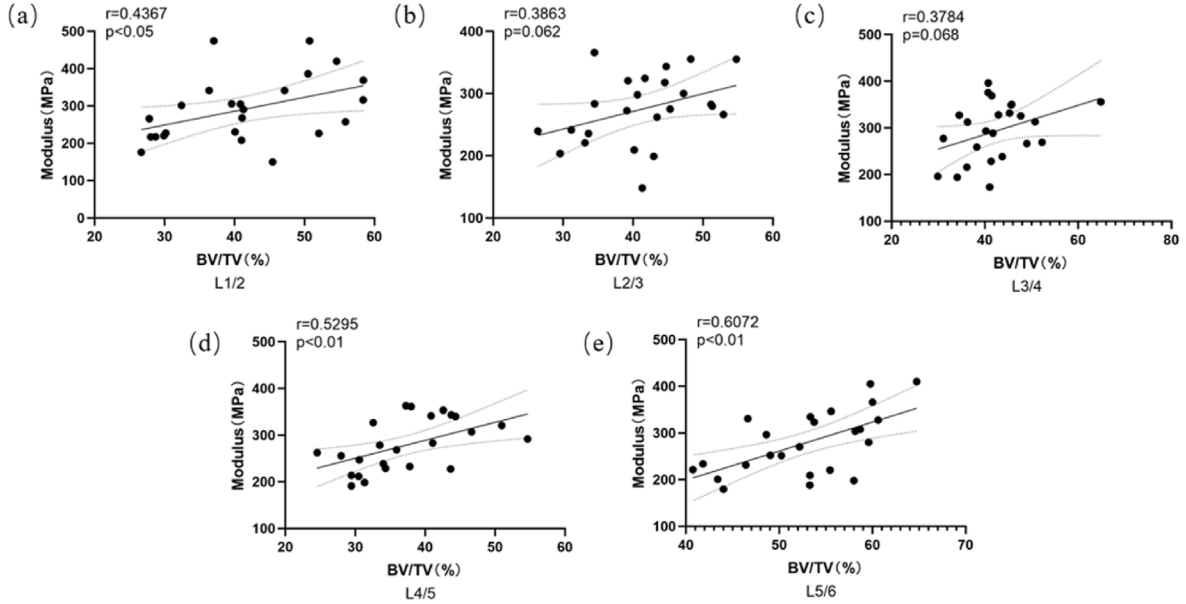

Fig. 15. The correlation between *E* and BV/TV of different segments.

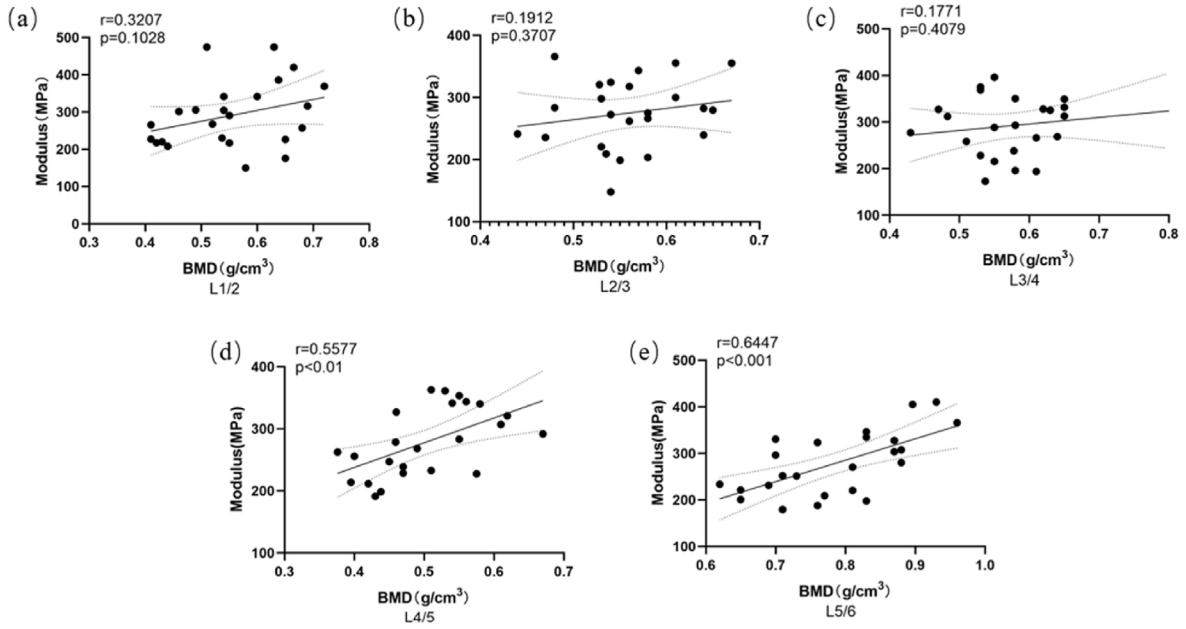

Fig. 16. The correlation between *E* and BMD of different segments.

corresponding regions inside the vertebral body endplate were observed. The mechanical parameters of endplate in the experimental group and the control group were obtained by indentation test, and the correlation between the bone mesoscopic structure and mechanical properties of endplate in the experimental group and the control group was analyzed. The imaging evaluation results showed that the height of the intervertebral space in the experimental group was significantly decreased, and the nucleus pulposus was dehydrated. The results of bone mesoscopic structure showed that the internal structure of the endplate was dense and the gap distance was reduced during intervertebral disc degeneration, which resulted in the narrowing of the internal channel structure of the endplate and had a negative impact on the nutrient supply of the intervertebral disc. The change of bone mesoscopic structure further affects the mechanical properties of the endplate, resulting in the enhancement of the mechanical properties of the vertebral endplate after intervertebral disc degeneration. The narrowing of the internal channel structure, hindering nutrition, which may be the key cause of intervertebral disc degeneration. It provides a biomechanical basis for studying the mechanism of intervertebral disc degeneration. In the future work, increasing the dynamic observation of nutrient transport in the process of intervertebral disc degeneration, combined with structural and mechanical observations will provide a better basis for exploring the mechanism of intervertebral disc degeneration.

Funding source

Thanks to the National Natural Science Foundation of China (11472185, 11972243) for funding!

Thanks to Fund Program for the Scientific Activities of Selected Returned Overseas Professionals in Shanxi Province (2020040) for funding

CRediT authorship contribution statement

Bingying Zhao: Writing – original draft. **Yuan Guo:** Writing – review & editing. **Xushu Zhang:** Data curation. **Yibo Zhao:** Methodology. **Bin Zhao:** Methodology. **Ming Zhang:** Methodology.

Declaration of competing interest

The authors declare that they have no known competing financial interests or personal relationships that could have appeared to influence the work reported in this paper.

References

[1] Adams MA, Hutton WC, Stott JR. The resistance to flexion of the lumbar intervertebral joint. Spine 1980;5(3):245–53. https://doi.org/10.1097/00007632-198005000-00007.

[2] Adams MA, Dolan P, Hutton WC. The lumbar spine in backward bending. Spine 1988;13(9):1019–26.

[3] Snuggs JW, Day RE, Bach F, Conner MT, Bunning RA, Tryfonidou MA, et al. Aquaporin expression in the human and canine intervertebral disc during maturation and degeneration. Jor Spine 2019;2(1):e1049. https://doi.org/10.1002/jsp2.1049.

[4] Iguchi T, Kanemura A, Kasahara K, Kurihara A, Doita M, Yoshiya S. Age distribution of three radiologic fambar instability: probable aging process of the instability with disc degeneration. Spine 2003;28(23):2628–33. https://doi.org/10.1097/01.BRS.0000097162.80495.66.

[5] Kang R, Li H, Ringgaard S. Interference in the endplate nutritional pathway causes intervertebral disc degeneration in animmature porcine model. Int Orthop 2014;38(5):1011–7. https://doi.org/10.1007/s00264-014-2319-9.

[6] Masuda K, Aota Y, Muehleman C, Imai Y, Okuma M, Thonar EJ. A novel rabbit model of mild, reproducible disc degeneration by an anulus needle puncture: correlation between the degree of disc injury and radiological and histological appearances of disc degeneration. Spine 2005;30(1):5–14. https://doi.org/10.1097/01.brs.0000148152.04401.20.

[7] Sun X, Jin WJ, Shen KP, Liu XZ. Degeneration of injured intervertebral disk affected by anterior longitudinal ligament destruction. Cjter 2017;21(11):1664–8.

[8] Hee HT, Chuah YJ, Tan BHM, Setiobudi T, Wong HK. Vascularization and morphological changes of the endplate after axial compression and distraction of the intervertebral disc. Spine 2011;36(7):505–11. https://doi.org/10.1097/BRS.0b013e3181d32410.

[9] Bai XD, Wang DL, Hou LS, Ge F, Xu C, Li W, et al. Upright posture combined with noninvasive axial loading-induced rabbit intervertebral disc degeneration. Chin J Spine Spinal Cord 2017;27(6):545–52.

[10] Yamaguchi T, Goto S, Nishigaki Y, Orias AAE, Bae WC, Masuda KInoue N. Microstructural analysis of three-dimensional canal network in the rabbit lumbar vertebral endplate. J Orthop Res 2015;33(2):270–6. https://doi.org/10.1002/jor.22759.

[11] Revel M, Andre-deshays Claudie, Roudier R, Roudier B, Hamard G, Amor B. Effects of repetitive strains on vertebral end plates in young rats. Clin Orthop Relat Res 1992;(279):303–9.

[12] Lotz JC, Colliou OK, Chin JR, Duncan NA, Liebenberg E. Compression-induced degeneration of the intervertebral disc: an in vivo mouse model and finite-element study. Spine 1998;23(23):2493~2506. https://doi.org/10.1097/00007632-199812010-00004.

[13] Schneiderman G , Flannigan B , Kingston S , Thomas J , Dillin WH , Watkins RG. Magnetic resonance imaging in the diagnosis of disc degeneration: correlation with discography. Spine1987; 12(3): 276-281..
[14] Grant J P, Oxland T R, Dvorak M F. Mapping the structural properties of the lumbosacral vertebral endplates.Spine2001;vol. 26(8): 889-896. https://doi.org/10.1097/00007632-200104150-00012..
[15] Cheng CC, Ordway NR, Zhang X, Lu YM, Fang H, Fayyazi AH. Loss of cervical endplate integrity following minimal surface preparation. Spine 2007;32(17): 1852–5. https://doi.org/10.1097/BRS.0b013e31811ece5a.
[16] Zhao F, Pollintine P, Hole BD, Dolan P, Adams MA. Discogenic origins of spinal instability. Spine 2005;30(23):2621–30. https://doi.org/10.1097/01.brs.0000187897.25889.54.
[17] Kim KS, Yoon ST, Li J, Park JS, Hutton WC. Disc degeneration in the rabbit: a biochemical and radiological comparison between four disc injury models. In: Spine, vol. 30; 2005. p. 33–7. https://doi.org/10.1097/01.brs.0000149191.02304.9b. 1.
[18] Thaler M, Hartmann S, Gstöttner M, Lechner R, Gabl M, Bach C. Footprint mismatch in total cervical disc arthroplasty.Eur Spine j013; 22(4): 759-765.https://doi.org/10.1097/01.brs.0000149191.02304.9b..
[19] Pharr GM, Oliver WC, Brotzen FR. On the generality of the relationship among contact stiffness, contact area, and elastic modulus during indentation. Jmr 1992; 7(3):613–7. https://doi.org/10.1557/JMR.1992.0613.
[20] Zhang SS. Composites and viscoelastic mechanics. Mech Ind Prss 2005.
[21] Briscoe BJ, Fiori L, Pelillo E. Nano-indentation of polymeric surfaces. J Phys D Appl Phys 1999;31(19):2395. https://doi.org/10.1088/0022-3727/31/19/006.
[22] Habelitz S, Marshall SJ, Marshall Jr GW, Balooch M. Mechanical properties of human dental enamel on the nanometre scale. Arch Oral Biol 2001;46(2):173–83. https://doi.org/10.1016/S0003-9969(00)00089-3.
[23] Rho JY, Zioupos P, Currey JD, Pharr GM. Variations in the individual thick lamellar properties within osteons by nanoindentation. Bone 1999;25(3):295–300. https://doi.org/10.1016/S8756-3282(99)00163-5.
[24] Griffith JF, Wang YXJ, Antonio GE, Choi KC, Yu A, Ahuja AT, et al. Modified pfirrmann grading system for lumbar intervertebral disc degeneration. Spine 2007; 32(24):E708–12. https://doi.org/10.1097/BRS.0b013e31815a59a0.
[25] Iorio JA, Jakoi AM, Singla A. Biomechanics of degenerative spinal disorders. Asian Spine J 2016;10(2):377. https://doi.org/10.4184/asj.2016.10.2.377.
[26] Abd EI, Aziz TA, Monamed RH, Hashem RM. Asso-ciation of lipoprotein lipase and apolipoprotein C-IIIgenes polymorphism with acute myocardial infarction indiabetic patients. Mol Cell Biochem 2011;354(1–2):141–50.
[27] Zhang XH, Xu HG, Wu TL. Disc degeneration and biomechanics. Ijos 2010;31(3): 137–8. https://doi.org/10.1155/2012/726210.
[28] Jing FJ, Zhan HS, Zhang J. Effects of manipulation on the ultrastructure of skeletal muscle in the model of cervical disc degeneration on rabbits. Orthop J China, 2005; (3):146–7.
[29] Kepler CK, Ponnappan RK, Tannoury CA, Risbud MV, Anderson DG. The molecular basis of intervertebral disc degeneration. Spine J 2013;13(3):318–30. https://doi.org/10.1016/j.spinee.2012.12.003.
[30] Zhu Q, Gao X, Levene HB, Brown MD, Gu W. Influences of nutrition supply and pathways on the degenerative patterns in human intervertebral disc. Spine 2016; 41(7):568. https://doi.org/10.1097/BRS.0000000000001292.
[31] Wang P, Wu J, Zheng C. The impact of nutrition and biomechanics of intervertebral disc degeneration. Ojc 2015;23(3):260–2.
[32] Pfirrmann CW, Metzdorf A, Zanetti M, Hodler J, Boos N. Magnetic resonance classification of lumbar intervertebral disc degeneration. Spine 2001;26(17): 1873–8. https://doi.org/10.1097/00007632-200109010-00011.
[33] Ruan D, He Q, Ding Y, Hou L, Li J, Luk KD. Intervertebral disc transplantation in the treatment of degenerative spine disease: a preliminary study. Lancet 2007; 369(9566):993–9. https://doi.org/10.1016/S0140-6736(07)60496-6.
[34] Zhao FD, Pollintine P, Hole BD, Adams MA, Dolan P. Vertebral fractures usually affect the cranial endplate because it is thinner and supported by less-dense trabecular bone. Bone 2009;44(2):372–9. https://doi.org/10.1016/j.bone.2008.10.048.
[35] Edwards w T, Zheng Y, Ferrara L A, Yuan H A. Structural features and thickness of the vertebral cortex in the thoracolumbar spine.Spine2001;vol. 26(2): 218-225.https://doi.org/10.1097/00007632-200101150-00019..
[36] Fields AJ, Costabal FS, Rodriguez AG, Lotz JC. Seeing double: a comparison of microstructure, biomechanical function, and adjacent disc health between double-layer and single-layer vertebral endplates. Spine 2012;37(21):E1310.
[37] Wang Y, Battié MC, Boyd SK, Videman T. The osseous endplates in lumbar vertebrae: thickness, bone mineral density and their associations with age and disk degeneration. Bone 2011;48(4):804–9. https://doi.org/10.1016/j.bone.2010.12.005.
[38] Oei L, Koromani F, Breda SJ, Schousboe JT, Clark EM, Meurs JBJV, et al. Osteoporotic vertebral fracture prevalence varies widely between qualitative and quantitative radiological assessment methods: the Rotterdam Study. J Bone Miner Rres 2018;33(4):560–8. https://doi.org/10.1002/jbmr.3220.
[39] Holmes A D, Hukins D W, Freemont A J. End-plate displacement during compression of lumbar vertebra-disc-vertebra segments and the mechanism of failure.Spine1993;vol. 18(1): 128-135.https://doi.org/10.1097/00007632-199301000-00019..
[40] Landham PR, Gilbert SJ, Baker-Rand HL, Pollintine P, Brown K, Adams M, et al. Pathogenesis of vertebral anterior wedge deformity: a 2-stage process? Spine 2015; 40(12):902–8. https://doi.org/10.1097/BRS.0000000000000905.
[41] Jackman TM, Hussein AI, Adams AM, Makhnejia KK, Morgan EF. Endplate deflection is a defining feature of vertebral fracture and is associated with properties of the underlying trabecular bone. J Orthop Res 2014;32(7):880–6. https://doi.org/10.1002/jor.22620.
[42] Fields AJ, Lee GL, Keaveny TM. Mechanisms of initial endplate failure in the human vertebral body. J Biomech 2010;43(16):3126–31. https://doi.org/10.1016/j.jbiomech.2010.08.002.
[43] Jackman TM, Hussein AI, Curtiss C, Fein PM, Camp A, De Barros L, Morgan EF. Quantitative, 3D visualization of the initiation and progression of vertebral fractures under compression and anterior flexion. J Bone Miner Res 2016;31(4): 777–88. https://doi.org/10.1002/jbmr.2749.
[44] Simpson EK, Parkinson IH, Manthey B, Fazzalari NL. Intervertebral disc disorganization is related to trabecular bone architecture in the lumbar spine. J Bone Miner Res 2001;16(4):681–7. https://doi.org/10.1359/jbmr.2001.16.4.681.
[45] Roberts S, McCall IW, Menage J, Haddaway MJ, Eisenstein SM. Does the thickness of the vertebral subchondral bone reflect the composition of the intervertebral disc? Eur Soine J 1997;6(6):385–9. https://doi.org/10.1007/BF01834064.
[46] Fazzalari N L, Manthey B, Parkinson I H. Intervertebral disc disorganisation and its relationship to age adjusted vertebral body morphometry and vertebral bone architecture. Anat Rec2001,vol. 262(3):331-339.https://doi.org/10.1002/1097-0185(20010301)262:3<331::AID-AR1044>3.0.CO;2-H..
[47] Zehra U, Robson-Brown K, Adams MA, Dolan P. Porosity and thickness of the vertebral endplate depend on local mechanical loading. Spine 2015;40(15): 1173–80. https://doi.org/10.1097/BRS.0000000000000925.
[48] Wang Y, Owoc JS, Boyd SK, Videman T, Battié MC. Regional variations in trabecular architecture of the lumbar vertebra: associations with age, disc degeneration and disc space narrowing. Bone 2013;56(2):249–54. https://doi.org/10.1016/j.bone.2013.06.022.
[49] Keller TS, Ziv I, Moeljanto E, Spengler DM. Interdependence of lumbar disc and subdiscal bone properties: a report of the normal and degenerated spine. J Spinal Disord Tech 1993;6(2):106–13.
[50] Zhang H, Cui L, Wang C, Zhihong WU, Yao J Qiu. G observation of vertebral endplates microstructure in a scoliosis rat model with asymmetric load by using micro CT. Chin J Bone Joint Surg 2015;8(5):429–33.
[51] Cheng C C, Ordway N R, Zhang X, Lu Y M, Fang H, Fayyazi A H. Loss of cervical endplate integrity following minimal surface preparation. Spine2007; vol. 32(17) 1852-1855. https://doi.org/10.1097/BRS.0b013e31811ece5a..
[52] Mulder L, Koolstra JH, den Toonder JM, van Eijden TM. Intratrabecular distribution of tissue stiffness and mineralization in developing trabecular bone. Bone 2007; 41(2):256–65. https://doi.org/10.1016/j.bone.2007.04.188.
[53] Hodgskinson R, Currey JD, Evans GP. Hardness, an indicator of the mechanical competence of cancellous bone. J Orthop Res 1989;7(5):754–8.